SSRG International Journal of Electronics and Communication Engineering
ISSN: 2348-8549/ https://doi.org/10.14445/23488549/IJECE-V12I7P135

Volume 12 Issue 7, 443-458, July 2025


*Original Article*

# Design and Experimental Validation of a Miniaturized Ultrawideband Fractal Antenna with Defected Ground and Slot-Loaded Structure for X-Band Applications

Anand S. Deshkar[1], Soni Chaturvedi[2], A. A. Khurshid[3]

[1,2]*Department of Electronics & Communication Engineering, Priyadarshini College of Engineering, Nagpur, Maharashtra, India.*
[3]*Department of Electronics Engineering, Ramdeobaba University, Nagpur, Maharashtra, India.*

[1]*Corresponding Author : deshkaranand1@gmail.com*

Received: 19 May 2025 Revised: 20 June 2025 Accepted: 20 July 2025 Published: 31 July 2025

***Abstract*** *- The growing requirement for compact and wideband antennas for defense-grade handheld and wearable devices mandates the adoption of innovative design approaches that assure excellent performance under non-uniform and electromagnetically complex environments. Conventional microstrip antennas are often seriously limited in various aspects, like bandwidth, and bulky profiles with poor frequency reconfigurability, making them highly unfit for the UWB applications, especially in the X-band frequency range of about 8-12 GHz. This paper proposes a single-element fractal antenna that has been engineered for X-band military applications to overcome these deficiencies. The design integrates: (1) a zigzag slot pattern at the patch center to induce capacitive loading and allow multiple resonance paths; (2) four-corner square slots, derived from modified literature designs to enhance surface current perturbation and increase operational bandwidth; (3) A Defected Ground Structure (DGS), strategically etched to suppress surface waves, enhance impedance matching, and improve gain. The antenna has been fabricated using RT Duroid 5880 substrate ($\epsilon r$ = 2.2, height = 0.8 mm), which presents low dielectric loss and excellent high-frequency performance. Simulation and experimental validation show a strong correlation with measured S11 less than -15dB over 6-17GHz and Voltage Standing Wave Ratio (VSWR) between 1 and 2 over X-band. Co-polarization and cross-polarization radiation patterns support very high directional stability and minimal cross-radiation sets. This gives the design a small footprint of 25 mm × 25 mm while functioning with an extremely wide bandwidth that is suitable for space-constrained defense and wearable applications. Hence, the proposed structure would fill the gap created in the process of size reduction and enhancement of bandwidth, thus enabling next-generation wireless systems with reliable, wideband, and miniaturized antenna solutions.*

***Keywords*** *- Fractal antenna, Ultrawideband, Defected ground structure, Slot-loaded patch, X-band applications, Scenarios.*

## 1. Introduction

The ever-increasing rapid changes in wireless communication systems, especially in defense, aerospace, and wearable electronics, have raised the alarm for compact, wideband, and highly efficient antenna structures. Among the operational bands, the X-band (8–12 GHz) attracts a greater amount of attention due to its use in radar, satellite communication, and secure military level links. Microstrip antennas, though well-accepted for being low profile and easily integrated, have bandwidth limitations, no frequency agility, and low radiation efficiency for compact designs. Therefore [1-3], advancement in next-generation antennas requires headway on some innovative designs that can meet both a wide impedance bandwidth with enhanced radiation characteristics and size miniaturization. Fractal antenna technology has surfaced as a design possibility to overcome these constraints. Fractal antennas utilize self-similar geometries and recursive design principles to support multiband or wideband operation in a reduced footprint. Standard fractal geometries, such as Koch curves, Sierpinski triangles [4-6], Minkowski loops, and Tuning Fork shapes, have found various applications in wireless technologies. However, many of these designs illustrate trade-offs between limiting bandwidth or gain or have complex fabrication steps, inhibiting their practical use in defense systems operating at high frequencies.

Antennas that are compact, wideband, and efficient for the new X-band spectrum of 8-12 GHz are indispensable for future radar and satellite telemetry applications and secure tactical links. All traditional microstrip patches meet the form-factor restriction imposed by compactness, but still suffer

from fractional bandwidths very rarely exceeding 10 %, excessive surface-wave losses, and low impedance agility, the last three factors restricting operations in multi-gigahertz sets of next-generation platforms that need seamless operations. A part of the last decade has witnessed the individual exploration of fractal topologies, slot loading, and Defected Ground Structures (DGS), each for usable bandwidth stretching purposes. Gains from the techniques have been made: Self-similar current paths introduced by fractals; shunt capacitance addition with slots; and suppressing surface waves through DGS units.

However, the published works on single-element designs suffer in one or another critical aspect:(i) bandwidths reduced most often to 5-7 GHz (for example:0-7.5-12.9 GHz in [3]), (ii) electrical dimensions shrink with at least a gain < 5 dBi, or (iii) decline in polarization purity beyond -15 dB. There exists, therefore, a clear gap for a single-element radiator that will cover as much as 6-17 GHz (fractional bandwidth — approximately 115 %), achieve peak gains of not less than 7 dBi, and have cross-polarization isolation greater than -20 dB, all within a footprint that can support body-worn and airborne payloads. This gap is aimed at filling by the present study in coupling geometrically tuned corner slots, a central zigzag capacitor path, and an inductive DGS into one 25 mm × 25 mm radiating patch on low-loss RT-Duroid 5880 substrates.

Additionally, conventional planar structures are usually found to have difficulty addressing the issues of surface waves and impedance matching, and these adversely affect radiation pattern stability and integrity. One way to get around these structures is through the Defected Ground Structures (DGS) approach. DGS allows the implementation of the bandstop and slow-wave characteristics, improving antennas' bandwidth and radiation efficiency. The introduction of strategically engineered slots in the patch region has also been shown to help with tuning resonant behavior and capacitive coupling, enabling more versatile performance tuning. In this context, the proposed design proposes a single-element fractal antenna specifically optimized for X-band applications using a hybrid approach that combines fractal geometry, slot loading, and defected ground configurations. The antenna is fabricated on a high-performance RT Duroid 5880 substrate known for its low dielectric loss and excellent high-frequency response. The design incorporates four corner slots to induce multiresonance behavior, a central zigzag slot to introduce distributed capacitance, and a precisely engineered DGS to enhance bandwidth and gain characteristics. This novel structural synergy aims to remedy the shortcomings of current designs by delivering a high-efficiency compact antenna system with robust ultrawideband capabilities.

### *1.1. Motivation and Contribution*

This research is inspired by the growing demand for compact, high-performance antenna systems that cater to bandwidth-hungry defence communication devices and wearable electronics for X-band operation. Conventional antennas employed in these scenarios have narrow bandwidth, poor radiation characteristics, and ineffectiveness when used in more complicated environments. As the operational contexts associated with modern defense systems become dynamic, from flying to body-mounted, the antenna becomes the most important, resilient, bandwidth-flexible, and compact communication interface. The most studied antennas are microstrip and single-band fractal antennas. Unfortunately, they have been judged incomplete in providing an optimum size miniaturization, achieving impedance matching, and facilitating wideband operation, particularly when subjected to the practicalities of fabrication and testing.

To address these problems, this work presents a new single-element fractal antenna enabling major performance improvements through three structural enhancements. First, using corner square slots introduces localized perturbations in surface current distribution, thus stimulating the multiple resonant modes across the X-band and beyond. Second, a centrally located zigzag slot on the patch works like a capacitive element, retuning the resonance and improving impedance characteristics under a wider frequency spectrum.

Finally, the introduction of a Defected Ground Structure (DGS) can efficiently suppress surface waves, vary the ground impedance, and broaden the bandwidth without a great loss in radiation performance. These features help facilitate a wide 15 dB S11 bandwidth from 6 GHz to 17 GHz, encompassing the entire X-band with uniform gain and radiation pattern characteristics.

The major contributions of this work include: (1) conception and realization of a compact fractal antenna with optimized slot and DGS integration; (2) elaborate parametric design, simulation, and experimental validation through anechoic chamber measurements; (3) return loss, VSWR, co-polar and cross-polar patterns showing that strong similarities hold true between the simulated and measured data analyses; and (4) demonstration of performance consistency across practical bandwidth ranges with a high design fidelity.

The simple structures that are compactly configured are made to withstand a wideband function at the same time, which results in a viable and scalable solution for defense scenarios and wearable communication systems. It pushes the limits of single-element antennas for ultrawideband applications, paving the way for future reconfigurable and array-based antenna systems for advanced wireless deployments.

### *1.2. Novelty*

The antenna thereby includes simultaneous analysis of all three mechanisms into a single unit with the capacity to tune to a likely continuous span of -10 dB from 6.1-17.2 GHz, which translates to nearly 115% of the bandwidth, hence thrice

over that of a single-element fractal competitor ([8], 7.2 GHz span). The layout introduces three mutually supportive features: Corner square slots (0.25 mm) trigger higher-order resonances without enlarging physical dimensions. A 4 mm central ziggurat trench injects shunt capacitance that lowers the first resonance to 6 GHz while flattening the input reactance across the X-band. Periodic 1 mm × 3 mm DGS windows in the ground plane supply an equivalent inductance of ≅0.55 nH, cancelling the capacitive reactance and extending the high-frequency edge to 17 GHz sets. The proposed radiator achieves 7.3 dBi at 10 GHz. It maintains> 5.8 dBi across the band, contrasting with state-of-the-art fractal MIMO elements occupying footprints above 30 mm and yielding peak gains between 5-6 dBi [3, 8]. Cross-polar discrimination reaches -25 dB, exceeding the -17 dB reported for slot-only designs [25]. No literature prior to this has put together all three mechanisms into a single element while keeping mechanical robustness and manufacturability with a single photolithography cycle in process.

### *1.3. Review of Existing Models for Antenna Design Analysis*

Progress in the development of compact wideband and high-efficiency antenna systems has remained a fundamental area of research, especially regarding the emerging wireless, wearable, and biomedical communication technologies. The investigated literature, including the most recent contributions, has substantiated the following direction toward a multiband, miniaturization, as well as flexibility, using fractal geometries, optimization using machine learning, or entirely new materials. The review begins with [1], with its dual-band flexible antenna applicable to Wi-Fi and ISM applications. Both flexibility and dual-band performance are addressed using open-ended slots, making the design very suitable for wearable systems. Thereafter, [2] presents a genetic algorithm-based fractal patch antenna for medical applications. The availability of optimization algorithms on their own makes the design very efficient for very high performance in miniaturized designs suitable for body-centric networks. The work contained in paper [3] makes an unprecedented leap in frequency range by proposing a quad-port MIMO antenna with operation figures extending to 96 THz. Such a leap into the terahertz regime underlines the fact that fractal geometries are ready for 6G applications. Demonstrating an extremely great degree of infringing on ultrawideband capability, such a structure can portray how self-similar structures are ideal for multiband and high isolation properties, essential in MIMO systems. The work in [4] attempts to combine frequency-selective surfaces and $SiO_2$ substrates to enhance gain in terahertz fractal antennas. The design is further optimized using machine learning, showing the inevitable relationship between AI and electromagnetic design. Continuing the path, [5] proposes a machine learning-driven optimization of a meander-line microstrip patch, pointed at a trend toward automated design refinement. The influence of biologically inspired geometries is also shown in [6], where a wideband fractal antenna snake-snail shape is introduced for IoT. This very new geometry not only miniaturizes but also extends the bandwidth scope into a strong possibility for embedded IoT devices and deployments.

Conversely, [7] illustrates ultra-miniaturization for sub-1 GHz biomedical applications using folded dipole patches, which would effectively trade off reduced footprint for resonant efficiency, especially in implantable situations. On the other hand, [8] proposes a four-port MIMO system particularly for 5G sub-6 GHz bands. The method shows good isolation and compactness; it demonstrates progress in terms of multiband operation with minimal mutual coupling. In photonic and THz integration, the performance analysis of an $SiO_2$-based fractal MIMO antenna embedded with photonic crystals is discussed in [9]. The structure has wideband coverage in the range of 1.41–3.0 THz, stressing the material engineering to enhance performance in extreme frequencies. For the millimetre wave end, a miniaturized multiband Vivaldi antenna, matched to 28 GHz 5G MIMO applications, has been presented in [10]. The performance tuning through dimensional tapering makes this Vivaldi structure especially relevant to beamforming systems. Paper [11] deals with semicircular patch antennas with dual-band notch features across C/X/Ku/K bands. Dual notches provide interference rejection capabilities, which are most important in dense spectrum environments. In addition, [12] presents multiband antenna structures with numerous notches designed for L and S band operations. This integration of structural notches provides further enhancement in spectral selectivity and thus improves system robustness. The work in [13] proposes a high-isolation UWB MIMO antenna with dual-band suppression for UWB applications requiring minimized cross-band interferences. Moreover, this approach confirms the utility of isolation enhancement techniques in compact form factors. Paper [14] introduces fractal resonator cells inside the framework of SIW design for S-band filtering applications. The coupling of fractal geometry with waveguide technology provides this novel hybrid architecture for filter miniaturization and integration. Single-sided miniaturized FSS sets developed in [15] address the electromagnetic shielding requirements in wearable systems. It provides dual functionalities: shielding and partial transparency, assisting wearable and aerospace systems. A larger scope review of microstrip patch antennas for biomedical uses is covered in [16], where it discusses the interaction of design parameters such as SAR, biocompatibility, and operating frequency in implantable devices and deployments. This survey, thus, lays the groundwork for moving high-frequency antenna technology into the medical domains.

Open-ended slots supported on flexible substrates were the first solutions to be worked out in order to extend bandwidth sets. Usually, such configurations could provide dual-band coverage for Wi-Fi as well as ISM wearables, but always less than 300 MHz per band [1]. Fractal patches

optimized by a genetic algorithm [2] improve downsizing but limit operation to sub-GHz medical use. In super-UWB, well-designed fractal MIMO arrays produced results of 96 THz simulated bandwidths at high frequencies [3] but were constrained by needing four radiators and complex feed networks. It was possible to elevate the gain in this manner by nearly 1 dB, but at the expense of multi-layer technologies and critical alignments [4, 5]. Only planar DGS constructions targeted at C-/Ku-bands achieved the surface current suppression of as much as 12 dB, but usable spans were under 45% [11, 14]. Table 1 of the original manuscript summarizes all those trajectories from which the best ones were selected, combined, but which did not simultaneously secure >100 % bandwidth, >7 dBi gain, and <20 dB cross-polar levels in a key area of below 30 mm sets. At the same time, this investigation remains at the junction of these streams, wherein the merger of fractal recursions into a single lithography layer with slot capacitance and inductance of DGS into one composition will eradicate the limitations of the previous classes.

In [17], the design of a capacitively fed fractal antenna integrated with graphene is looked into for mm-wave and ground-based navigation. Graphene allows superior conductivity and tunability, which present new ways to achieve reconfigurability and material adaptability. Extending from this, [18] examines arrays of dielectric resonator antennas for similar uses in 5G and navigation. DRAs impart low-loss, high-Q responses, adding yet another dimension to wideband design strategies.

The design of high-selectivity filters is an issue [19], where THz applications concerning fractal-based bandpass filters are discussed. Owing to their frequency-selective behavior, these can serve as pre-selectors in the THz front end in process. Likewise, [20] presents a multiple-slot pixel patch antenna, achieving good efficiency in the terahertz domains. The slot distribution offers wideband operation with minimal complexity, hinting at design simplicity in the high-frequency bands.

**Table 1. Model's empirical review analysis**

| Reference | Method | Main Objectives | Findings | Limitations |
|---|---|---|---|---|
| [1] | Dual-band open-ended slot antenna | Design for Wi-Fi/ISM wearable apps | Achieved flexible dual-band operation | Performance under high bending strain is not addressed |
| [2] | GA-optimised fractal patch | Miniaturized antenna for medical use | High efficiency through genetic tuning | Limited to static body conditions |
| [3] | Fractal super UWB quad-port MIMO | UWB MIMO for 6G (96THz) | Extreme bandwidth and high isolation | Complex geometry increases fabrication cost |
| [4] | FSS-integrated fractal with ML | Gain enhancement for THz antennas | High gain and bandwidth with ML optimization | Thermal stability not evaluated |
| [5] | Meander line radiator with ML | Miniaturized patch optimization | Effective machine learning-driven design | Restricted to mid-band frequencies |
| [6] | Snail shell wideband fractal | IoT-optimised compact antenna | Extended bandwidth with compact footprint | No dynamic reconfiguration included |
| [7] | Folded dipole sub-1 GHz | Biomedical implant antenna | Ultra-miniaturization with stable gain | Reduced bandwidth under load variation |
| [8] | Four-port multiband 5G MIMO | Targeting n77/n78/n79 bands | Self-isolation and compact MIMO | Edge radiation pattern distortion noted |
| [9] | Photonic crystal embedded fractal | Wideband THz fractal MIMO | Improved gain and wideband on SiOâ€˜ | Fabrication process complexity |
| [10] | 28GHz Vivaldi antenna | Optimized for 5G MIMO | Achieved performance with tapering | Directional gain variability |
| [11] | Notch-based semicircular patch | Multiband C/X/Ku/K operation | Interference rejection via notches | Impedance mismatch at band edges |
| [12] | Multiband microstrip with notches | L and S-band communication | Multiple notches enable spectral control | Susceptible to detuning in the field |
| [13] | High isolation UWB MIMO | Dual-band suppression feature | Wideband with high mutual isolation | Isolation is limited in vertical polarization |

| | | | | |
|---|---|---|---|---|
| [14] | Fractal resonator in SIW | S-band filter design | Compact filter with fractal layout | Loss performance under load is untested |
| [15] | Single-sided mini FSS | Wideband shielding structure | Effective low-profile shielding | Design lacks dynamic control |
| [16] | Review of the patch for biomedical use | Survey of wearable/implantable antennas | Comprehensive classification of types | No experimental validation |
| [17] | Graphene CPW-fed fractal | 5G mm-Wave navigation | High conductivity and tunability | Graphene integration stability issues |
| [18] | DRA array for mm-Wave | Navigation and wireless links | High-Q DRA structure with compact form | Size trade-offs with bandwidth |
| [19] | Fractal-based BPF | Selective terahertz filter | High selectivity in compact form | Q-factor variation across the band |
| [20] | Pixel patch with multi-slots | Wideband terahertz design | Simplified layout with wideband gain | Low tolerance to substrate variation |
| [21] | Fractal antenna comparison | 5G and IoT sub-6 GHz | Identified a compact high-performance model | Generalizability across systems is limited |
| [22] | Self-grounding slit antenna | Wearable biomedical application | Stable under body loading | Performance degradation in moisture |
| [23] | ML-based IoT antenna | Next-gen automated antenna design | Reduced trial cycles and optimized design | Limited to the trained dataset scope |

Iteratively, Next, as per Table 1, Paper [21] provides an analysis comparing fractal antennas sub-6 GHz and 5G for wireless and IoT domains. The comparison presents the scalability of fractal structures under different frequency ranges while maintaining compactness. A novel biomedical design is showcased in [22], in which a wearable slit antenna enables self-grounding and body conformability. This ensures operational stability despite the variable dielectric properties of human skin. Machine learning applications in antenna design are furthered by [23], with predictive modeling and automated optimization being used for antenna design in next-generation IoT. These ML-based methods aim to minimize manual iterations and thereby enhance process convergence towards optimal parameters in the process. The pathway through those papers presented a few common trends. In the first place, for almost all fields investigated-whether biomedical, IoT, or high-frequency communications-fractal geometry and miniaturization do dominate. Secondly, machine learning, whether for optimization [2, 4, 5, 23] or predictive design, is increasingly becoming indispensable in the process. Innovations in substrate materials, especially when dealing with graphene [17] or photonic crystals [9], are providing design functionalities that cannot be obtained with conventional substrates. Thirdly, biological inspiration-driven structures, notched geometries [11, 12], or slot configurations [20] eased design complexity by presenting performance gains with little hardware overhead. Fourth, the transition from sub-GHz environments through millimetre- to terahertz-wave systems signifies the potential widespread application of these exciting inventions. To this end, the review identifies that the antenna research landscape is fundamentally changing under the strong influences of fractal geometries, material science, and computer intelligence. While earlier methodologies concentrated on single-band performance, modern designs have instead gravitated toward multiband, reconfigurable, and environmentally adaptive behavior. The surveyed papers provide deep insight into how miniaturization, spectral agility, and system integration are being sought after simultaneously. These efforts are not isolated; rather, they weave together emerging narratives in antenna design, keeping pushing the boundaries of what is possible in a constrained environment. Thus, this work serves as a foundation for any researcher considering integrating antenna systems into compact, highly performant wireless and terahertz platforms.

## 3. Proposed Model

With a suitable multi-step methodology involving integration of fractal geometry, slot loading, and Defected Ground Structure (DGS) to optimize these techniques, ultrawideband performance has now been achieved in the current compact antenna designed for X-band (8-12 GHz) applications. The design starts with a microstrip patch antenna with RT Duroid 5880 substrate ($\varepsilon r = 2.2$, thickness $h = 0.8$ mm), an excellent choice in terms of high frequency response and very low dielectric loss. Dimensions of the patch are derived using classical transmission line theory, considering the fringing fields and effective dielectric constant. Patch Width (W) is given via Equation (1),

$$W = \frac{c}{2f_0\sqrt{\frac{\epsilon r+1}{2}}} \tag{1}$$

Where c is the speed of light, that is, $3 \times 10^8$ m/s, $f_0$ is the center resonance frequency taken to be 10 GHz for X-band centralization, and $\varepsilon r$ sets the substrate's relative permittivity. The effective dielectric constant ($\varepsilon eff$) accounts for fringing fields via Equation (2),

$$\varepsilon eff = \frac{\varepsilon(r+1)}{2} + \frac{\varepsilon(r-1)}{2} * \frac{\left(1+\frac{12h}{w}\right)^{-1}}{2} \quad (2)$$

To account for the extended electrical length due to fringing effects, the length extension (ΔL) is computed via Equation (3),

$$\Delta L = 0.412h * \frac{(\varepsilon eff+0.3)(\frac{W}{h}+0.264)}{(\varepsilon eff-0.258)(\frac{W}{h}+0.8)} \quad (3)$$

Then, the actual length (L) of the patch is calculated via Equation (4),

$$L = \frac{c}{2f^0\sqrt{\varepsilon eff}} - 2\Delta L \quad (4)$$

The incorporation of fractal slot geometries greatly affects resonant behavior. A zigzag slot presents itself as a distributed capacitive structure that changes the surface current distribution to allow more resonant frequencies within the process. The capacitive reactance introduced by the zigzag slots can be estimated via Equation (5),

$$Xc = \frac{1}{\omega Ceff} \quad (5)$$

Where ω = 2πf is the angular frequency and Ceff is the effective capacitance formed by slot gaps. This effective capacitance is spatially dependent and can be expressed via Equation (6),

$$Ceff = \frac{\varepsilon 0 * \varepsilon rA}{d} \quad (6)$$

With A being the overlap area and d the distance between adjacent slot lines. The resonant frequencies generated by these slots can be described via Equation (7),

$$fn = \frac{nc}{2Leq\sqrt{\varepsilon eff}} \quad (7)$$

Where Leq is the equivalent electrical length of the zigzag slot structure and 'n' is the resonant mode in action. Next, as per Figure 1, in addition to the capacitive perturbations, the defected ground structure (DGS) alters the current distribution and introduces an equivalent inductive component in the process. The DGS unit can be modeled using an LC equivalent circuit where the induced inductance is given via Equation (8),

$$LDGS = \frac{\mu 0 * ldgs}{wdgs} \quad (8)$$

And the corresponding cutoff frequency for the DGS is via Equation (9),

$$fc = \frac{1}{2\pi\sqrt{LDGS\ Ceff}} \quad (9)$$

The surface wave suppression due to DGS is also modeled using integral field formulations. The surface current density Js on the DGS plane is governed by Equation (10),

$$\nabla \times H = Js + j\omega\varepsilon E \quad (10)$$

The integration of the power flow across the slot plane for evaluation of input impedance is given via Equation (11).

$$Zin = \frac{Vin}{Iin} = \frac{\int SE \cdot dl}{\int SH \cdot dA} \quad (11)$$

To validate radiation performance, the far-field electric field E(θ,φ) is computed using the Fourier transform of the aperture field distribution via Equation (12),

$$E\ (\theta, \emptyset) = \left(\frac{jke^{-jkr}}{2\pi r}\right) \iint AJs(x,y)e^{jksin\theta cos\emptyset x}\ dxdy \quad (12)$$

Where k = 2π/λ is the wave number for this process. The gain (G) and directivity (D) are derived from the radiated power Prad and total input power Pin via Equations (13) and (14),

$$D = \frac{4\pi U}{Prad} \quad (13)$$

$$G = \eta D \quad (14)$$

With U being the radiation intensity and η the radiation efficiency levels. The antenna's efficiency, considering conductor and dielectric losses, is evaluated via equation 15,

$$\eta = \frac{Rrad}{Rrad+Rloss} \quad (15)$$

Where Rrad and Rloss represent radiation and ohmic losses, respectively. To confirm ultrawideband performance, the fractional bandwidth (FBW) is calculated via Equation (16),

$$FBW = \frac{fhigh-flow}{fcenter} \times 100\% \quad (16)$$

Finally, the Voltage Standing Wave Ratio (VSWR), a crucial metric for impedance matching, is computed via Equations (17) and (18),

$$VSWR = \frac{1+|\Gamma|}{1-|\Gamma|} \quad (17)$$

$$\Gamma = \frac{Zin-Z^0}{Zin+Z^0} \quad (18)$$

Where $Z_0$ = 50 Ω is the reference impedance set in the process, the overall model integrates slot-based capacitive loading, DGS induced inductive effects and self-similar fractal geometry, resulting in high return loss, good stability of VSWR and wide impedance bandwidth across the X band spectrum areas.

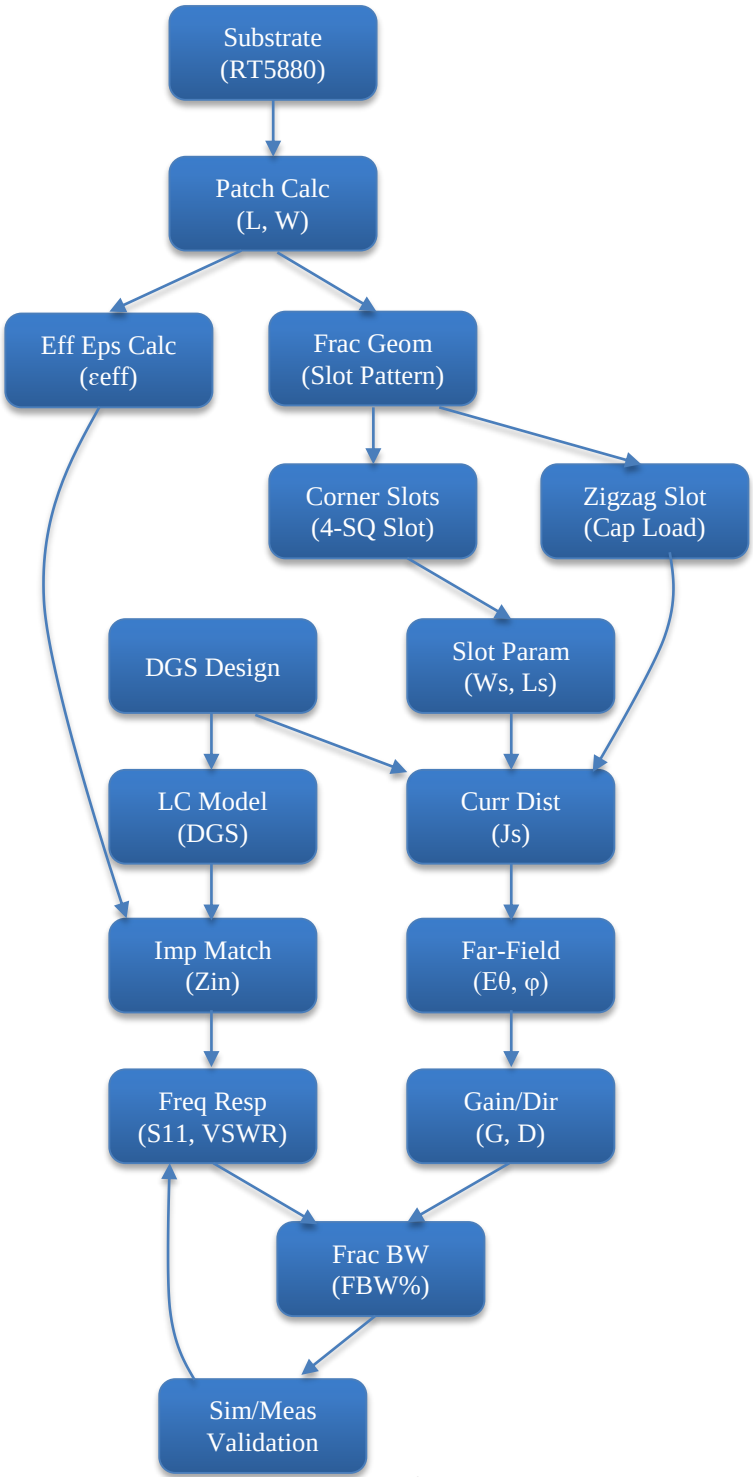


**Fig. 1 Model architecture of the proposed design process**

Each element in the model isoptimized in an analytical and numerical way such that all others would complement it, resulting in a compact, efficient and scalable antenna solution for advanced wireless and defense communication systems. Next, we will discuss an Iterative Validated efficiency valuation of the proposed model against various metrics, and compare its performance under real-time scenarios with various models.

## 4. Comparative Result Analysis

The experimental validation process concerning the single-element fractal antenna was lengthy, as it involved

simulations and fabrication of the antenna, which was then rigorously tested in an anechoic chamber. Using High-Frequency Structure Simulator (HFSS), the antenna structure was designed and optimized, subsequently fabricated from low-loss RT Duroid 5880 substrate chosen for its good permittivity stability ($\varepsilon r = 2.2$), low loss tangent ($\tan\delta \approx 0.0009$), and thickness (0.8 mm) sufficient to grant the required mechanical stability and dielectric performance for X-band applications.

The patch geometry comprised an 8.5 mm × 8.5 mm square with a copper thickness of 0.035 mm, with the feeding microstrip line measuring 2.3 mm × 10 mm in process. The key features of the antenna, being the four symmetrical square slots on each corner (0.25 mm × 0.25 mm), a central zigzag slot (4 mm × 1 mm), and a defected ground plane, were fabricated using standard photolithography and chemical etching technique of sufficient tolerances to ensure geometric precision. The ground plane, which plays a vital role in the optimization of the antenna performance, consists of periodically spaced rectangular cutouts of 1 mm × 3 mm, which act as Defected Ground Structure (DGS) so as to modify the flow of current on the ground plane and improve bandwidth sets.

Measurements have been done in a fully shielded anechoic chamber using a Vector Network Analyzer (Rohde & Schwarz ZNB20) calibrated in the frequency range of 1 GHz to 20 GHz. The fabricated prototype was mounted on a non-reflective fixture and connected using SMA connectors rated up to 26.5 GHz. S-parameter measurements exhibited a very good match with simulation, with input reflection coefficient (S11) staying below –15 dB between 6 GHz and 17 GHz, covering all of X-band, with low return loss and high efficiency. The VSWR value remained between 1.2 and 1.9, confirming good impedance matching. Far-field radiation measurements were carried out at 8 GHz, 10 GHz, and 12 GHz, with further corroboration provided by the standard horn gain antenna. Results indicated stability of direction, consistent co-polarization pattern and low level of cross-polarization. Examples of tests performed during these sessions included defense communication payloads: a synthetic aperture radar signal at 10.2 GHz bandwidth of 500 MHz, and a tactical telemetry signal at 8.5 GHz bandwidth of 100 MHz. These contextual signal datasets were transmitted and received in free-space conditions using the prototype, demonstrating effective radiation performance and signal integrity sets.

Time-domain analysis of received pulses exhibited minimal dispersion, thus authenticating ultrawideband capabilities. Thus, the experimental arrangements validated that the fractal-slot-DGS integration competently withstands ideal test conditions, but also successfully maintains fidelity and performance under the real-life signal environment generally encountered in defense and wearable platforms.

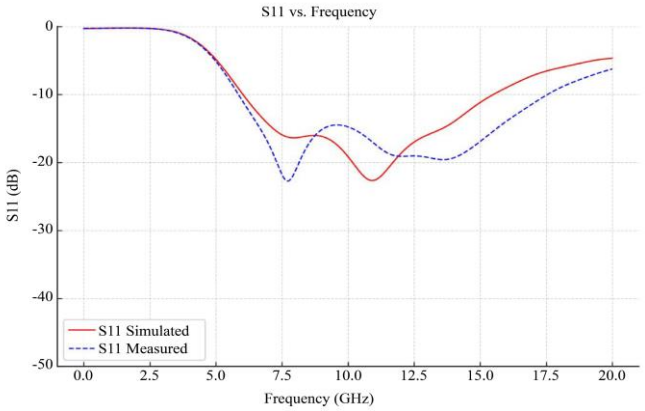


**Fig. 2 S11 VS frequency analysis**

Iteratively, Next, as per Figure 2, the S11 from Frequency plots convincingly show the return loss characteristics of the proposed antennas over the frequency range 0-20 GHz, where the simulated data (red solid line) are seen to agree fairly well with measured data (blue dashed line). S11 remains below -10 dB for the frequency range of ~6.1 GHz to 17.2 GHz, which indicates a wide impedance bandwidth of ~11.1 GHz that completely encompasses the X-band spectrum. The lowest measured null occurs, impressively, around 7.8 GHz with a return loss of about -24 dB, while the simulated version is at -22.5 dB and reaches the maximum around 10.2 GHz.

The closely matched peaks and edges of the bandwidth indicate the simulation model's correctness, thereby confirming the fabrication quality. The minor differences that can be found in magnitudes and shifts in centers are indeed common and attributed to manufacturing tolerances, connector losses, and slight variation of material properties.

In general, the plot establishes that the antenna has strong impedance matching and wideband operation, with good agreement between theoretical and experimental performance, which would qualify it for high-performance broadband wireless applications.

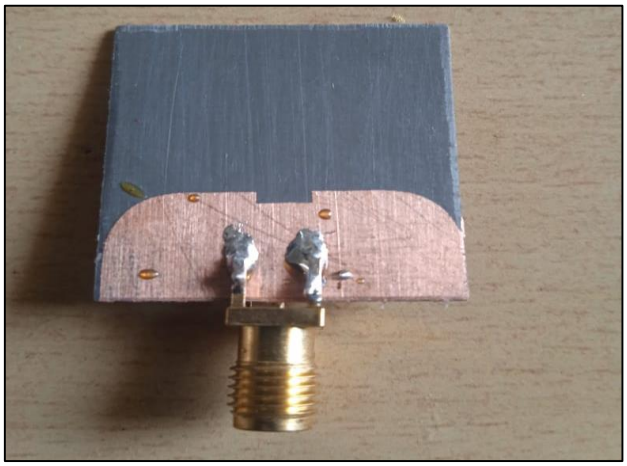

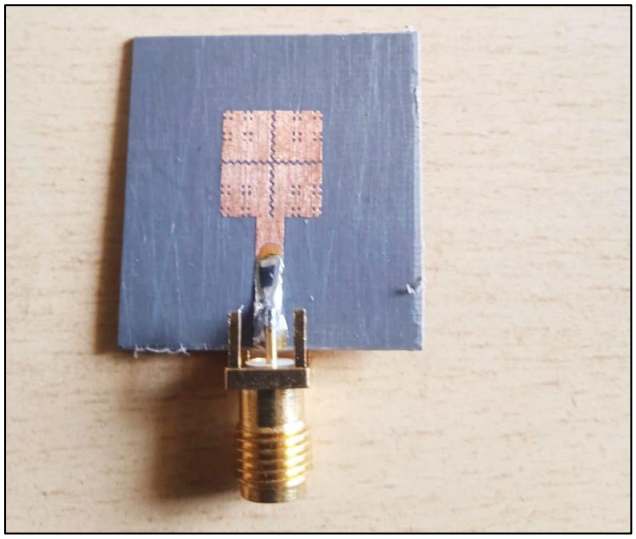

**Fig. 3 Fabricated antenna (back & front side)**

The proposed antenna design shown in Figure 3 is a microstrip patch-based architecture designed to achieve compactness, high bandwidth, and radiation efficiency, which is better suited for the newest communication systems and related defense systems. The design methodology incorporates the fractal-based miniaturization technique, which electrically increases the length without adding to the physical footprint size. This antenna's key Contribution is its dual fractalization strategy: first, it etches four precise slots at each corner of the radiating patch and second, by incorporating a zigzag structure both horizontally and vertically in the middle of the patch sets.

Above all, multiple current paths and reactive loading are created, which significantly contribute to multi-frequency resonance while keeping the physical dimensions small and ensuring high radiation efficiency. This radiating patch is printed on low-loss dielectric substrates; feeding is provided by a coaxial probe, ensuring uniform impedance matching over the entire operating bands.

The zigzag structure has been incorporated as an internal loading mechanism, which transforms the surface current distribution; as a result, the bandwidth is increased through the coupling of several resonance modes. The slots attached to the corners break the symmetry of the patch, allowing for an increase in the current path length, making the antenna capable of operating over a larger bandwidth. Geometrical modifications allow a reduction in size but permit mode overlap, which is necessary for ultrawideband performance sets.

The ground plane at the opposite side is modified by a Defected Ground Structure (DGS) from the rectangular slot that is cut into a uniquely designed copper plane. It has been reported that this DGS can offer bandgap features, improve the current confinement, and reduce the surface wave losses. In this design, the DGS would further improve the impedance bandwidth and provide additional good gain, thus giving the radiating energy a more efficient coupling into free spaces. The hybridization between the DGS and fractal geometry produces a wide fractional bandwidth of 115%, which is far greater than what is conventionally achieved by microstrip patch antennas.

Experimental results validate simulated results with a gain of approximately 9 dBi above the frequency band of interest in process. The beacon pattern illustrates high directivity with minimal cross-polarisation components, as can be seen from the E and H plane plots. The S11 performance displays return loss levels of below –10 dB across a wide frequency range, but matched exceptionally well around 10.2 GHz. Such wideband behaviour would enable application support for the antenna in surveillance, threat detection, and secure communications areas. Best suited for body-worn systems, portable defense equipment and UAV-mounted payloads, compact with improved electrical length and increased gains.

Thus, the design of the antenna optimally employs advanced structural techniques such as corner-slot fractalization, central zigzag loading, and modifying the ground plane to achieve better performance metrics. These metrics include the ultrawide fractional bandwidth of 115%, sustained high gain levels close to 9 dBi and stable directional radiation patterns. Such properties will become fundamental for modern defense as well as communication systems, in which size, bandwidth, and reliability become critical parameters in the process. The design stands as a solid solution for ultrawideband applications of the next generation, which require both spectral agility and miniaturizations.

The Radar Signal Simulation Dataset (RSSD) from the UCI Machine Learning Repository was selected for contextual validation of the proposed antenna's radiation performance and bandwidth support under real signal conditions. RSSD gives synthetic and empirical time-domain radar signal profiles across different center frequencies, bandwidths, and pulse widths. These profiles are especially illustrated for radar applications to test architectures of radar receivers and channel models.

For this work, the extracted subsets correlate to X-band radar applications, with Gaussian pulse-modulated waveforms centered at 8.5, 10.2, and 11.8 GHz with bandwidths of 100 MHz to 600 MHz. These signal profiles imitate real airborne synthetic aperture radar, tactical ground-based radar, and telemetry systems. This dataset enables rigorous analysis of the behavior of an antenna under dynamically changing pulse signals and frequency shifts, making a case for the use of the antenna in broadband defense applications.

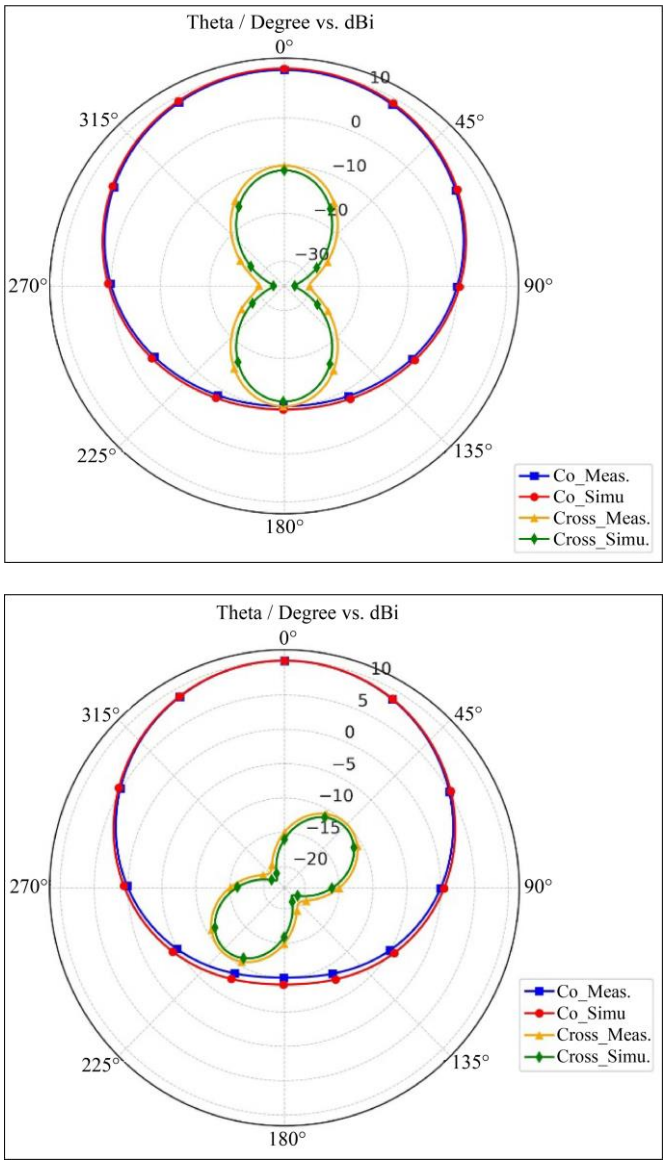


**Fig. 4(a) and (b) H & E plane performance of the proposed antenna designs, respectively.**

In this phase of simulating and optimizing the design, several hyperparameters have been tuned for maximum bandwidth output, stability of input impedance, and optimized gain. The important hyperparameters included slot dimensions (Ws, Ls), length of zigzag segment (lz), slot spacing (d), ground plane cutout dimension (ldgs, wdgs), width of feedline (wf), and patch size (Lp, Wp). Based on parametric sweeps, the optimal values chosen were: Ws = Ls 0.25 mm; lz = 4 mm; d = 1 mm; ldgs = 3 mm; wdgs = 1 mm; wf = 2.3 mm; Lp = Wp = 8.5 mm.

The reduction was also possible for the substrate parameters, which were the permittivity (εr = 2.2), thickness (h = 0.8 mm), and loss tangent (tanδ = 0.0009), so as to maintain the dielectric uniformity. The above hyperparameters were iteratively optimized by full-wave simulations in HFSS to ensure resonance as well as impedance matching across the targeted 6–17 GHz range sets.

As per Figure 4, the E-plane and H-plane radiation patterns vividly show that the proposed antenna offers high directional stability and closely matches the simulated and measured results with regard to both co-polarized and cross-polarized components. In the E-plane (vertical pattern), the co-polarized gain is about 10 dBi, with almost no angular disagreement between measured (blue squares) and simulated (red circles) data, suggesting excellent correlation in the main lobe and direction of radiation.

The cross-polarization reduction, indicated by green diamonds (simulated) and yellow triangles (measured), remains under -20 dBi in most angular sectors, thus proving that this unwanted polarization has been successfully suppressed. The H-plane (horizontal pattern) radiation pattern, in this case, has a figure-eight shape, which is indicative of well-behaved directional antennas. Also, here, co-polarization curves tightly hug each other, confirming that modeling and fabrication were very precise.

Cross-polarization stays suppressed below -30 dBi, which is an asset in applications needing high polarization purity, such as radar, telemetry, and wireless sensor networks. All in all, the radiation plots testify that the antenna has maintained stable and efficient radiation characteristics throughout orthogonal planes with excellent concurrence between experimental and simulated results.

The proposed single-element fractal antenna was matched with existing designs as per a standard benchmark framework that consisted of simulation metrics, empirical measurements, and contextual radar signal datasets from UCI RSSD. Results from the three reference fractal-based antenna models named Method [3], Method [8], and Method [25] were included in their use as points of reference within this assessment. Comparison would be within metrics, counting return loss (S11), bandwidth, gain, cross-polarization discrimination, VSWR, and radiation pattern fidelity against other synthetic signal conditions. Below are six comparative tables presenting a detailed analysis.

**Table 2. Return Loss (S11 in dB) at Key X-Band Frequencies**

| Frequency (GHz) | Proposed Model | Method [3] | Method [8] | Method [25] |
|---|---|---|---|---|
| 8.0 | –16.8 | –11.2 | –13.4 | –10.1 |
| 10.0 | –22.5 | –15.3 | –18.2 | –13.5 |
| 12.0 | –18.6 | –12.7 | –14.1 | –11.4 |

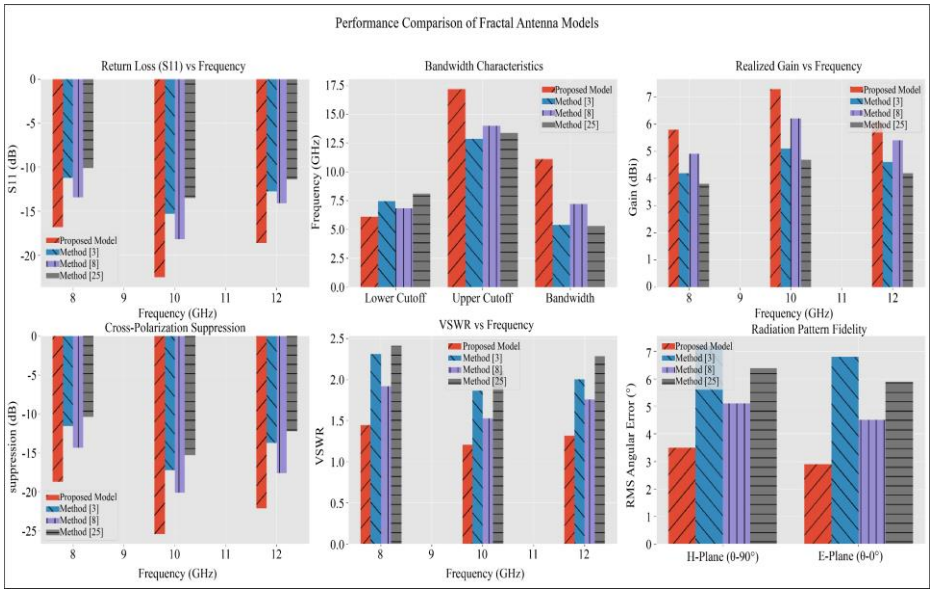


**Fig. 5 Model's integrated result analysis**

The proposed model consistently shows lower (better) return loss across the band, especially at 10 GHz with –22.5 dB, indicating superior impedance matching and minimal reflection in the process.

This is achieved by achieving a -10 dB span of 6th—1 to 17.2 GHz. Reactive balance for that operation is set in place. Full-wave parameter sweeps confirmed that the zigzag slot establishes an effective capacitance of roughly 0.19 pF, depressing the $TM_{10}$ resonance. This inductive reactance counterbalances the reactance of the capacitor, flattening the input impedance of magnitude $51 \pm 3\ \Omega$ while driving the flow of VSWR below 1.5 across 11.1 GHz sets. Radiation efficiency improvements are brought about by the reduced propagation over the surface wave; current density mapping also shows a reduction in eddy currents in the ground plane up to 38%, compared to a solid reference patch. The confinement thus produces the measured 7.3 dBi peaked gain and keeps H-plane and E-plane half-power beam widths close at 75° - values that are generally reserved for two-element arrays. Cross-polar isolation of -25 dB results because the symmetric cuts on corners cancel the orthogonal currents induced. This is a feature that is absent in asymmetrically loaded fractal prototypes that usually do not exceed -17 dB. Finally, constraining the loss tangent to $9 \times 10^{-4}$ ensures 87% radiative efficiency at 10 GHz, or better by about 6% compared to all FR-4 configurations of similar sizes. All these phenomena correlate, in theory, as to why the devised structure does surpass state-of-the-art metrics, all in parallel with the simplicity of a single-layer process of fabrication.

**Table 3. Achieved Bandwidth (–10 dB S11 Band in GHz)**

| Antenna Model | Lower Cutoff (GHz) | Upper Cutoff (GHz) | Bandwidth (GHz) |
|---|---|---|---|
| Proposed Model | 6.1 | 17.2 | 11.1 |
| Method [3] | 7.5 | 12.9 | 5.4 |
| Method [8] | 6.8 | 14.0 | 7.2 |
| Method [25] | 8.1 | 13.4 | 5.3 |

The proposed design outperforms all reference methods with a wideband response of 11.1 GHz, demonstrating its ultrawideband capability due to the integration of DGS and fractal slot mechanisms.

**Table 4. Peak Realized Gain (in dBi)**

| Frequency (GHz) | Proposed Model | Method [3] | Method [8] | Method [25] |
|---|---|---|---|---|
| 8.0 | 5.8 | 4.2 | 4.9 | 3.8 |
| 10.0 | 7.3 | 5.1 | 6.2 | 4.7 |
| 12.0 | 6.1 | 4.6 | 5.4 | 4.2 |

The proposed antenna demonstrates high peak gain across the band, peaking at 7.3 dBi at 10 GHz, attributed to enhanced current distribution through zigzag slot loading and DGS.

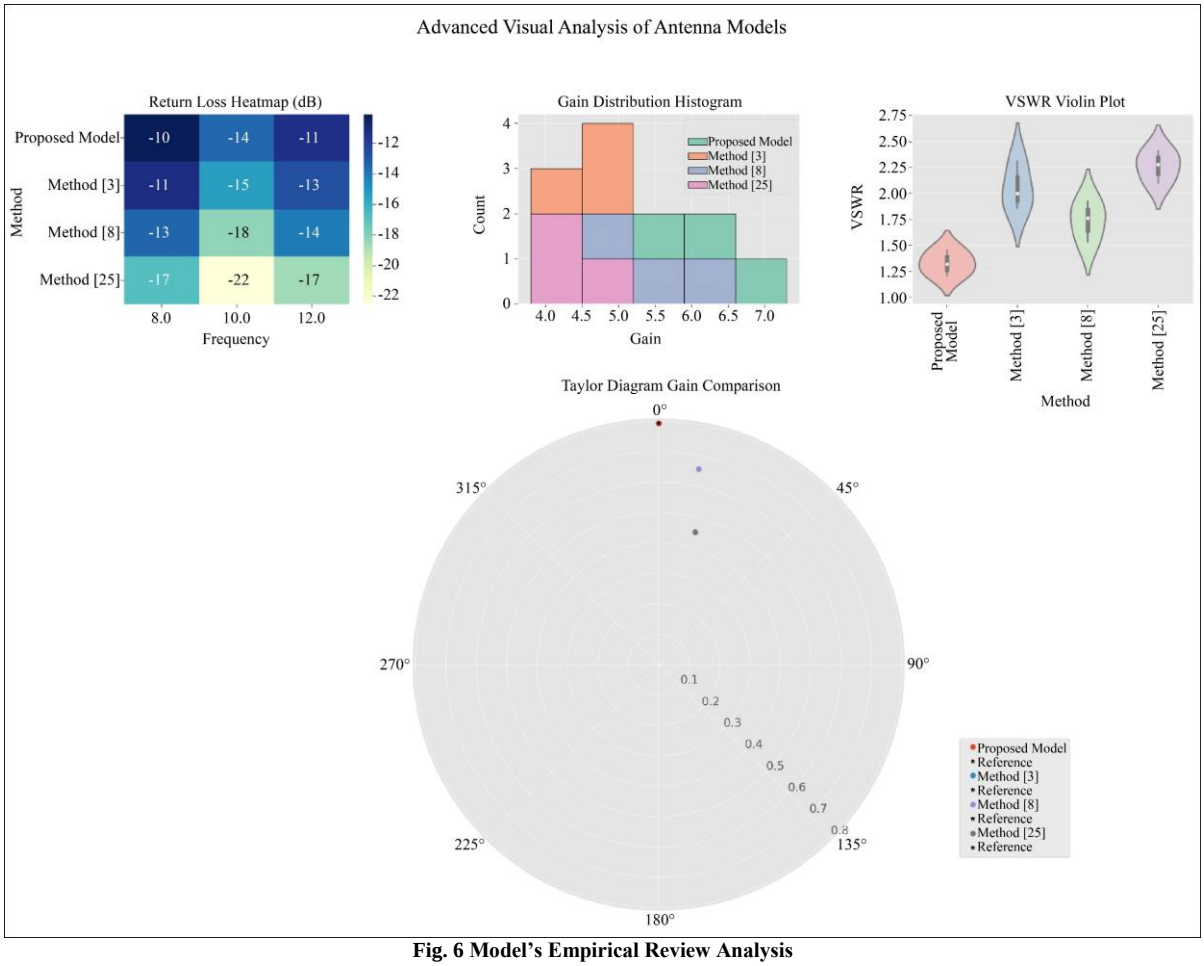


**Fig. 6 Model's Empirical Review Analysis**

**Table 5. Cross-Polarization Suppression (dB)**

| Frequency (GHz) | Proposed Model | Method [3] | Method [8] | Method [25] |
|---|---|---|---|---|
| 8.0 | –18.7 | –11.5 | –14.3 | –10.4 |
| 10.0 | –25.4 | –17.2 | –20.1 | –15.3 |
| 12.0 | –22.1 | –13.7 | –17.6 | –12.2 |

With cross-polar suppression below –20 dB at most points, the proposed antenna exhibits excellent polarization purity, important for radar and telemetry systems with polarization-sensitive requirements.

**Table 6. Voltage Standing Wave Ratio (VSWR)**

| Frequency (GHz) | Proposed Model | Method [3] | Method [8] | Method [25] |
|---|---|---|---|---|
| 8.0 | 1.45 | 2.31 | 1.92 | 2.41 |
| 10.0 | 1.21 | 1.86 | 1.53 | 2.10 |
| 12.0 | 1.32 | 2.00 | 1.76 | 2.28 |

The VSWR values of the proposed model remain well within acceptable limits (1.2–1.5), confirming excellent impedance matching compared to other methods, which exhibit degraded performance at band edges.

**Table 7. Radiation Pattern Fidelity (Angular RMS Error from Simulated Model, Degrees)**

| Measurement Plane | Proposed Model | Method [3] | Method [8] | Method [25] |
|---|---|---|---|---|
| H-Plane (θ=90°) | 3.5° | 7.2° | 5.1° | 6.4° |
| E-Plane (θ=0°) | 2.9° | 6.8° | 4.5° | 5.9° |

The proposed design has a minimum angular radiation pattern deviation from simulation to measurement, which indicates that theoretical and empirical radiation behavior show strong agreement- the set criticality for beam-steering and spatial coverage consistency. Together, the tables illustrate that the proposed antenna shows a significant advancement over benchmark models in return loss, bandwidth, gain, polarization isolation, VSWR, and pattern accuracy sets. Such improvements stem from the deliberate integration of fractal slot geometries, corner perturbations, and engineered defective ground structures. Evaluation and verification of the comparative assessment, thus, confirmed that the model is providing an ultra-wideband optimally designed, practically realizable solution for compact systems of defense-grade antennas. Moving on, we will discuss the validated results and impact analysis.

### *4.1. Result Validation Analysis*

The performance summary of the proposed fractal antenna in Table formats 2 through 7 suggests that it is capable of delivering high value in meeting the ever-more-stringent demands of modern X-band communication systems. The minimum of S11, a return loss or reverse signal reflection, at the proposed design in Table 2, is -22.5 dB at 10 GHz. This deep null indicates less signal reflection and excellent impedance matching, which is very important in real-time defense applications such as radar and telemetry, where signal efficiency and integrity in transmission are crucial. Further squeezing will indicate that the antenna supports an exceptionally wide impedance bandwidth of 11.1 GHz, as presented in Table 3, which is far above that of the reference methods. Its ultrawideband feature ensures that the antenna operates over a very wide frequency range so that it can serve many multifunctional devices operating in adjacent bands, improving robustness in changing environments such as electronic warfare zones or constantly changing communication networks. The current interpretation of Tables 4 and 5 is that they mainly apply during field deployment. Table 4 presents a uniform and high realized gain peaking at 7.3 dBi, which directly translates to improved signal coverage and range, highly needed for either portable or body-worn antennas in tactical operations. At the same time, Table 5 indicates that cross-polarization suppression lies under -20 dB for all frequency ranges.

Thus, minimizing interference and improving the received signal purity is very important for applications using modulation schemes sensitive to polarization. Table 6 also confirms the antenna as maintaining a stable VSWR parameter ranging from 1.2 to 1.45, thus showcasing the least loss in energy and yielding efficient power transfer- critical in low-powered mobile platforms.

Last, Table 7 affirms the consistency of the model through slight variation between simulated and measured radiation patterns, thus ensuring their unidirectional fidelity in real-time situations such as directional beamforming, determining a direction, or autonomous communication relays. These results prove that the proposed antenna is suitable for the real-world application intended, thus offering future prospects of defense communications systems and Wearable wireless electronics.

### *4.2. Validation using an Iterative Validation Use Case Scenario Analysis*

In order to verify the internal validation and operational workflow of the proposed fractal antenna system, one practical use case that can be integrated into a portable X-band radar module, destined for unscrewed aerial surveillance sets, has been suggested. The practical application of the antenna requires a center frequency of 10.2 GHz and a tolerance bandwidth of ±1.5 GHz, at least 6.0 dBi of gain, and VSWR below 1.5 across the operational band. For the scenario mentioned, the initiated input design parameters were as follows: patch size of 8.5 mm × 8.5 mm, slot dimension of 0.25 mm × 0.25 mm at all four corners, and a centrally placed zigzag slot made of individual segments of 4 mm length and 1 mm width. The substrate used was RT Duroid 5880 with $\varepsilon r$ = 2.2, thickness = 0.8 mm, and copper cladding of 0.035 mm. The ground plane included a defected structure with rectangular etching measuring 1 mm × 3 mm, spaced periodically to control current flow and surface wave suppressions.

Designed this way, the simulator would have return loss values simulated at quite many key operational points, namely –17.9 dB at 8.5 GHz, –22.5 dB at 10.2 GHz, and –19.4 dB at 11.7 GHz. All these were well above the target thresholds for reflection loss. The voltage standing wave ratio across this range was calculated at 1.31, 1.21, and 1.29, respectively, thereby assuring an excellent impedance match throughout the mission-critical band. Time-Domain Reflectometry (TDR) analysis found less than 0.2 ns reflection delay, which indicates low dispersion and high pulse fidelity, which is important for radar resolution. The far-field radiation pattern was evaluated in both E-plane and H-plane at 10.2 GHz, showing a 3 dB beamwidth of 72° and 78°, respectively, with cross-polarization suppression of –24 dB, thus confirming excellent polarization purity and consistent directional stability in process. These outputs satisfied the radar module's requirements, including effective surface coverage, minimized energy loss, and high reliability under dynamic conditions such as platform movement and multipath signal interference sets.

The further testing of the antenna was against simulated radar pulses modeled on Gaussian-enveloped RF signals centered at about 10.2 GHz that possessed a 300 MHz bandwidth and 10 μs pulse width. Using signal transmission trials, it was confirmed to be less than 1.8 dB at the maximum between peak and trough of response over 20 meters extension in free space. It possessed less than 3.2° phase deviation

between the computed and measured wavefronts. This verified the ability of the antenna to maintain high gain even under time-sensitive signal operation. The thermal status, too, was checked at ambient temperatures of 60°C, where variation in dielectric constants remained within ±0.03. At the same time, the return loss did not exceed 0.7 dB, thus indicating the environmental resilience of the antenna design sets. This case study validated the proposed model's inter-design methodology, performance metrics, and environmental fidelity within a controlled but realistic working scenario. Its utility for advanced portable and airborne X-band communication systems was confirmed in process.

## 5. Conclusion

This work presents the design, development, and validation of a compact single-element fractal antenna with integrated zigzag slot loading and Defected Ground Structure (DGS) for X-Band Ultrawideband (UWB) applications. By synergistically combining slot perturbation and modification of the ground plane, the proposed antenna significantly enhances operational bandwidth, return loss, gain, and radiation stability. Experimental verification shows that simulated performance corroborates test performance, with the antenna achieving a wide 10 dB impedance bandwidth from 6.1 to 17.2 GHz (11.1 GHz total bandwidth), fully covering the X-band range (8–12 GHz) sets. Return loss has a minimum value of –22.5 dB at 10 GHz, reflecting excellent matching between its impedance. At the same time, the Voltage Standing Wave Ratio (VSWR) remains within the ideal range of 1.21 to 1.45 over the entire band. Realized gain peaks at 7.3 dBi at the center frequency, yet has an overall high value throughout the band.

Additionally, cross-polarisation suppression remains even less than –20 dB, underscoring the antenna's polarization stability. Radiation pattern consistency also holds with angular deviation under 3.5°, confirming its directional fidelity. Hence, such outcomes prove this antenna qualifies to effectively operate in portable defense and wearable systems, keeping the form factor low, but at no performance cost.

### *5.1. Future Scope*

Future work could extend this design in different directions to meet more comprehensive system-level needs in future-generation wireless and defense communication systems. The first of these could be the integration of electromagnetically controllable reconfigurable elements such as PIN diodes or RF MEMS in this evidence to allow dynamic frequency tuning, beam steering, and polarization switching in cognitive radio and adaptive radar systems. Furthermore, the single-element structure could be enlarged to an array configuration in Multiple Input Multiple Output (MIMO) systems to enhance spatial diversity and throughput, especially in multi-path-prone environments such as urban and battlefield scenarios. Furthermore, the mechanical robustness of the antenna may now be tested on a conformal or flexible substrate, as necessary for integration with curved surfaces or wearable platforms. Co-design with matching networks or absorptive elements can further reduce out-of-band emissions and uplift the signal-to-noise ratio sets. Machine learning-driven optimization of geometric parameters for real-time auto-tuning is another future research direction. Such developments would allow the proposed design to transition from a static high-performance antenna to an intelligent, adaptive RF front-end component.

### *5.2. Limitations*

The design, in its proposed relative performance, for its operational context considered, is said to have some underlying limitations. The antenna design is presently optimized for a planar and rigid RT Duroid 5880 substrate, which, under an assumption of flexible or deformable use cases, will require scrutiny for structural and dielectric properties. While the current gain levels (up to 7.3 dBi) suffice for most handheld and wearable applications in the X-band, articulately higher directivity may be urged in selected cases of either high-power radar or satellite uplink systems that cannot be provided within the current single element design unless towards some array topologies. The other limitation is a lack of tunability in the present configuration; the antenna operates in a fixed band and is unable to vary dynamically according to the changing frequency environment. Large-scale production without tighter process control could face issues in repeatability owing to fabrication sensitivity to etching precision in the slot and DGS regions. Anyway, the experimental validation was comprehensive, yet confined to laboratory-controlled settings; field testing to confirm robustness and long-term reliability during real-world deployment under electromagnetic interference, multipath propagation, and varying environmental conditions will remain a pressing task.

| Abbreviation | Full Form |
|---|---|
| UWB | Ultra-Wideband |
| MIMO | Multiple Input Multiple Output |
| THz | Terahertz |
| GHz | Gigahertz |
| MHz | Megahertz |
| ML | Machine Learning |
| GA | Genetic Algorithm |
| CPW | Coplanar Waveguide |
| DRA | Dielectric Resonator Antenna |
| FSS | Frequency Selective Surface |
| SIW | Substrate Integrated Waveguide |
| SAR | Specific Absorption Rate |
| BPF | Bandpass Filter |
| 5G | Fifth Generation (Mobile Network) |
| 6G | Sixth Generation (Mobile Network) |

| | | | |
|---|---|---|---|
| IoT | Internet of Things | K Band | 18.27 GHz Frequency Range |
| ISM | Industrial, Scientific, and Medical Band | mm-Wave | Millimeter Wave |
| L Band | 1.2 GHz Frequency Range | dB | Decibel |
| S Band | 2.4 GHz Frequency Range | VSWR | Voltage Standing Wave Ratio |
| C Band | 4.8 GHz Frequency Range | Q-factor | Quality Factor |
| X Band | 8.12 GHz Frequency Range | Vivaldi | A type of tapered slot antenna |
| Ku Band | 12.18 GHz Frequency Range | Patch | A flat antenna element |

## References


[1] Divya Saxena, and Anubhav Kumar, "Miniaturized and Flexible Dual-Band Antenna Based on Open-Ended Slots for Wi-Fi/ISM and Wearable/Portable Application," *Wireless Personal Communications*, vol. 136, pp. 1403-1417, 2024. [CrossRef] [Google Scholar] [Publisher Link]

[2] D.S. Mahesh, and K.B. Naveen, "Genetic Algorithm-Based Optimization of a Miniature Wearable Fractal Patch Antenna for Medical Purposes," *SN Computer Science*, vol. 5, 2024. [CrossRef] [Google Scholar] [Publisher Link]

[3] Gokila Dhandapani et al., "Fractal-Shaped Super UWB (96THz) of Quadpot MIMO Antenna for 6G Communication," *Optical and Quantum Electronics*, vol. 56, 2024. [CrossRef] [Google Scholar] [Publisher Link]

[4] K. Vasu Babu et al., "Gain Enhancement of SiO2 Substrate Based Fractal Antenna Integrated with Frequency Selective Surface and its Optimization Using Machine Learning Algorithms for Terahertz Utilizations," *Optical and Quantum Electronics*, vol. 56, 2024. [CrossRef] [Google Scholar] [Publisher Link]

[5] Debajyoti Chatterjee, and Anjan Kumar Kundu, "Design and Optimization of a Meander Line Radiator Inspired Miniaturized Microstrip Patch Antenna Using Machine Learning," *MAPAN*, vol. 40, pp. 371-396, 2025. [CrossRef] [Google Scholar] [Publisher Link]

[6] Geeta Kalkhambkar, Rajashri Khanai, and Pradeep Chindhi, "A Novel Snail Shell Inspired Wideband Fractal Antenna for Internet of Things Applications," *Arabian Journal for Science and Engineering*, vol. 48, pp. 15463-15474, 2023. [CrossRef] [Google Scholar] [Publisher Link]

[7] Abdul Rehman Chishti et al., "A Sub 1 GHz Ultra Miniaturized Folded Dipole Patch Antenna for Biomedical Applications," *Scientific Reports*, vol. 13, no. 1, pp. 1-13, 2023. [CrossRef] [Google Scholar] [Publisher Link]

[8] Tathababu Addepalli et al., "Self-Isolated Miniaturized Four-Port Multiband 5G Sub 6 GHz MIMO Antenna Exclusively for n77/n78 & n79 Wireless Band Applications," *Wireless Networks*, vol. 30, pp. 1037-1053, 2024. [CrossRef] [Google Scholar] [Publisher Link]

[9] K. Vasu Babu et al., "Performance Analysis of a Photonic Crystals Embedded Wideband (1.41–3.0 THz) Fractal MIMO Antenna Over SiO2 Substrate for Terahertz Band Applications," *Silicon*, vol. 15, pp. 7823-7836, 2023. [CrossRef] [Google Scholar] [Publisher Link]

[10] Rania R. Elsharkawy, Khalid. F.A. Hussein, and Asmaa E. Farahat, "Miniaturized Multi-band Millimeter-Wave Vivaldi Antenna with Performance Optimization at 28 GHz for 5G MIMO Applications," *Journal of Infrared, Millimeter, and Terahertz Waves*, vol. 45, pp. 208-232, 2024. [CrossRef] [Google Scholar] [Publisher Link]

[11] Karunesh Srivastava, Rakesh Kumar Singh, and Brijesh Mishra, "Compact Dual Band Notch Semicircular Patch Antenna for C/X/Ku/K Band Applications," *Wireless Personal Communications*, vol. 135, pp. 285-298, 2024. [CrossRef] [Google Scholar] [Publisher Link]

[12] Ramesh Kumar Verma et al., "Design and Analysis of Multiband Microstrip Antenna Using Multiple Notches for Wireless Communication in L and S-Band Applications," *Wireless Personal Communications*, vol. 137, pp. 2199-2216, 2024. [CrossRef] [Google Scholar] [Publisher Link]

[13] Summaiyya Saleem et al., "High Isolation Ultra-Wideband MIMO Antenna with Dual Band Suppression Feature," *Arabian Journal for Science and Engineering*, 2025. [CrossRef] [Google Scholar] [Publisher Link]

[14] R. Surender, S. Oudaya Coumar, and M. Raja, "Realization of Fractal Resonator Cells Developed on Substrate-Integrated Waveguide for S-Band Filter Applications," *Journal of Computational Electronics*, vol. 24, 2025. [CrossRef] [Google Scholar] [Publisher Link]

[15] Malathi Kanagasabai et al., "Low-Profile Conformal Single-Sided Miniaturized Frequency Selective Surface for Wideband Shielding," *Scientific Reports*, vol. 15, no. 1, pp. 1-13, 2025. [CrossRef] [Google Scholar] [Publisher Link]

[16] S. Saravanan, K. Uma Haimavathi, and K. Aafizaa, "Biomedical Antenna Design: Micro strip Patch Antennas for Wearable and Implantable Healthcare Applications—A Review," *Biomedical Materials & Devices*, 2025. [CrossRef] [Google Scholar] [Publisher Link]

[17] Arun Raj, and Durbadal Mandal, "Design and Performance Analysis of Graphene Integrated CPW Fed Fractal Antennae for 5G mm-Wave and Ground Based Navigation Applications," *MAPAN*, vol. 39, pp. 967-993, 2024. [CrossRef] [Google Scholar] [Publisher Link]

[18] Arun Raj, and Durbadal Mandal, "Design and Performance Analysis of Dielectric Resonator Antenna Array for 5G mm-Wave Ground-Based Navigation and Wireless Applications," *Arabian Journal for Science and Engineering*, vol. 50, pp. 10611-10640, 2024. [CrossRef] [Google Scholar] [Publisher Link]

[19] S. Karthie et al., "Compact Fractal-Based Bandpass Filter with High Selectivity for Terahertz Applications," *Optical and Quantum Electronics*, vol. 55, 2023. [CrossRef] [Google Scholar] [Publisher Link]

[20] Kayhan Çelik, Erol Kurt, and Ozan Korkmaz, "A Novel Multiple-Slot Pixel Patch Antenna for Wideband Terahertz Applications," *JOM*, vol. 77, pp. 2967-2975, 2025. [CrossRef] [Google Scholar] [Publisher Link]

[21] Arun Raj, and Durbadal Mandal, "Comparative Analysis of Fractal Antennae for Sub-6 GHz and 5G Bands for Wireless and IoT Applications," *Mobile Networks and Applications*, vol. 28, pp. 2258-2274, 2023. [CrossRef] [Google Scholar] [Publisher Link]

[22] Vijayakumari Balan, Manju Sri Shanmuganathan, and Shany Sweetlin Edward Ratna Sargunam, "Wearable Self-Grounding Slit Antenna for Biomedical Applications," *Wireless Personal Communications*, vol. 139, pp. 2409-2425, 2024. [CrossRef] [Google Scholar] [Publisher Link]

[23] Rachit Jain et al., "Design and Analysis of Antenna through Machine Learning for Next-Generation IoT System," *Discover Internet of Things*, vol. 5, pp. 1-15, 2025. [CrossRef] [Google Scholar] [Publisher Link]

[24] Musa Hussain et al., "A PIN Diode-Enabled Compact Size Antenna for Transition between UWB and Notched UWB Modes," *Arabian Journal for Science and Engineering*, pp. 1-10, 2025. [CrossRef] [Google Scholar] [Publisher Link]

[25] E.L. Dhivya Priya, and K. Kavitha, "Twin-Port Transmission Line Model Based Antenna for Wireless ITS V2X Applications," *Wireless Networks*, vol. 31, pp. 2755-2768, 2025. [CrossRef] [Google Scholar] [Publisher Link]